Rare Metal Materials and Engineering
Volume 51, Issue 2, February 2022
Available online at www.rmme.ac.cn

Science Press

Cite this article as: Cui Shushan, Zhang Lei, Fa Tao. Phase-Field Simulation of Thermoelastic Martensitic Transformation in U-Nb Shape Memory Alloys[J]. Rare Metal Materials and Engineering, 2022, 51(02): 452-460.

ARTICLE

Phase-Field Simulation of Thermoelastic Martensitic Transformation in U-Nb Shape Memory Alloys

Cui Shushan, Zhang Lei, Fa Tao

Institute of Materials, China Academy of Engineering Physics, Jiangyou 621907, China

Abstract: Metastable α''-phase U-Nb shape memory alloys exhibit outstanding corrosion resistance and mechanical property, in which multi-level twinning martensite is the typical microstructure. Phase-field method was used to simulate the formation process of α'' thermoelastic martensite. Results show that driven by minimization of elastic strain energy, various self-accommodated martensite clusters are obtained, and several self-accommodation modes are found. Comparing the simulated results with experimental results, it is suggested that the asymmetric deformation gradient tensor and interface compatibility notably influence the variant pair and twinning plane. In addition, the texture development upon deformation was predicted based on the variant rearrangement process.

Key words: U-Nb alloy; martensitic transformation; phase-field model

Thermoelastic martensitic transformation (TMT) plays a key role in shape memory alloys (SMAs), because many outstanding properties of SMAs stem from TMT, such as the shape memory effect, the superelastic behavior and the elastocaloric effect[1-3]. TMT has some characteristics that differ from other solid-state phase transformations. For example, TMT is diffusion-free and shear-dominated, can be induced either by temperature changing or by stress loading, and the phase interfaces, i.e. the interfaces between martensite and parent phase or between different martensitic variants, exhibit good migration ability[4]. Owing to the transition from a high-symmetry phase to a low-symmetry phase, several thermodynamically equivalent variants with different crystal orientations are expected to occur. Actually, multi-variant microstructures are usually found in SMAs, including twinned lamellar martensite[5-7], V-shaped, triangular and hexangular martensites[7-9], herring-bone martensite[10], etc. It is generally accepted that the formation of multi-variant martensite is caused by minimization of elastic strain energy resulted from the transformation strain, i.e. the self-accommodation effect[7].

Owing to their good corrosion resistance and mechanical properties, U-Nb alloys are widely used in the field of nuclear engineering[11-13]. The shape memory effect of polycrystalline U-Nb alloy has been observed for several decades[14]. The composition range of Nb was 9at%~15at%. Upon quenching, the γ-phase with body-centered cubic (bcc) structure will transform without diffusion to the metastable α''-phase with monoclinic structure. Then, other evidences were found to support the standpoint that this transformation belongs to TMT, such as small volume change[15], low hysteresis of transformation temperature between direct and reverse transformations[16], and highly twinned martensite[17]. Based on the crystallography model of phase transformation proposed by Hatt[18], there are 12 martensitic variants for the $\gamma \rightarrow \alpha''$ transformation. The characteristics of transformation twins and the variant rearrangement phenomenon were revealed by transmission electron microscopy[19, 20]. The microstructure consists of parallel twinned bands, and the finely twinned bands are either (021) or $(\bar{1}30)$. Despite these experimental results, the detailed formation process of α'' martensite and the mechanism of specific twinning modes remain to be thoroughly investigated.

Currently, phase-field method has been widely used to simulate the microstructure formation in materials during solidification and solid-state phase transformations[21-24]. As the transformation eigen-strain and elastic strain energy are taken into account, the phase-field model of martensitic transformation was successfully applied to investigate the self-

Received date: February 23, 2021
Foundation item: National Natural Science Foundation of China (51701191)
Corresponding author: Fa Tao, Ph. D., Associate Professor, Institute of Materials, China Academy of Engineering Physics, Jiangyou 621907, P. R. China, Tel: 0086-816-3626742, E-mail: fatao@caep.cn

accommodation effect in several SMAs[25-27]. However, these simulation studies do not involve the $\gamma \rightarrow \alpha''$ TMT in U-Nb SMAs. In order to clearly elucidate the micro-mechanism of $\gamma \rightarrow \alpha''$ transformation, we applied the phase-field approach to investigate the formation process of α'' thermoelastic martensite (TM).

1 Phase-Field Model

The phase-field model of martensitic transformation is based on the model proposed by Wang and Khachaturyan[28]. Although an intermediate phase γ^o exists between the high-temperature γ-phase and the low-temperature α''-phase, it is supposed that the existence of γ^o slightly influences the martensite morphology[29]. Therefore, we ignored the γ^o phase in the present model. A set of order parameters ($\eta_p(x, t)$, p=1, 2, … , n) was used to distinguish the parent phase and the martensitic variants, e.g., η_p=1 and others equal to 0 represent variant p, and all η_p equal to 0 represents the parent phase. n is the number of variants. The microstructure evolution is governed by the time-dependent Ginzburg-Landau equation:

$$\frac{\partial \eta_p}{\partial t} = -L\frac{\delta G}{\delta \eta_p} \tag{1}$$

where L is the kinetic coefficient, G is the free energy of the system, which is divided to three parts: the bulk chemical energy (G_{ch}), the gradient energy (G_{gr}), and the elastic strain energy (G_{el}), i.e.

$$G=G_{ch}+G_{gr}+G_{el} \tag{2}$$

G_{ch} is governed by a fourth-order polynomial approximation:

$$G_{ch}=\int_V \left[\begin{array}{l}\frac{A}{2}\sum_{p=1}^{n}\eta_p^2-\frac{B}{3}\sum_{p=1}^{n}\eta_p^3+\frac{C}{4}\sum_{p=1}^{n}\eta_p^4\\ +\frac{D}{2}\sum_{p=1}^{n}\eta_p^2\left(\sum_{q=1}^{n,q\neq p}\eta_q^2\right)\end{array}\right]\mathrm{d}V \tag{3}$$

The last term in Eq. (3) is added to avoid coexistence of more than one variant at one material point. The coefficients A, B, C and D are determined by the chemical driving force and the energy barrier between different phases or different variants, A=32ΔG*, B=3A−12ΔG_m, C=2A−12ΔG_m. ΔG* is the energy barrier, and ΔG_m is the driving force.

The gradient energy can be represented by

$$G_{gr}=\int_V \frac{\beta}{2}\sum_{p=1}^{n}\left(\nabla\eta_p\right)^2\mathrm{d}V \tag{4}$$

where β is the gradient energy coefficient, determined by the interface energy and the energy barrier.

The elastic strain energy is calculated by

$$\begin{aligned}G_{el}&=\frac{1}{2}\int_V C_{ijkl}\varepsilon_{ij}^{el}\varepsilon_{kl}^{el}\mathrm{d}V\\&=\frac{1}{2}\int_V C_{ijkl}\left(\varepsilon_{ij}-\varepsilon_{ij}^0\right)\left(\varepsilon_{kl}-\varepsilon_{kl}^0\right)\mathrm{d}V\end{aligned} \tag{5}$$

where C_{ijkl} is the tensor of elastic constants, ε_{ij} is the strain tensor, ε_{ij}^{el} is the elastic strain tensor, and ε_{ij}^{0} is the eigen-strain tensor. Owing to the change of crystal structure and lattice parameter, TMT is accompanied with obvious transformation strain, i.e. the source of eigen-strain:

$$\varepsilon_{ij}^0=\sum_{p=1}^{n}\varepsilon_{ij}^{00}(p)\eta_p \tag{6}$$

where $\varepsilon_{ij}^{00}(p)$ is the transformation strain tensor of variant p, calculated from the lattice parameters and orientation relationship between the parent and martensite phases. The total and elastic strain fields are obtained by solving the mechanical equilibrium equation. Here we used the Khachaturyan-Shatalov microelasticity theory to calculate the strain field. More details of the calculation process can be found in Ref.[10].

In this study, the lattice parameters of γ and α'' phases were chosen as a_γ=0.346 nm, $a_{\alpha''}$=0.2909 nm, $b_{\alpha''}$=0.5751 nm, $c_{\alpha''}$=0.4977 nm, and $\gamma_{\alpha''}$=92.41°[29]. The orientation relationship between the parent and martensite phases[30] is

$[100]_{\alpha''}\leftrightarrow<111>_\gamma$, $\{010\}_{\alpha''}\leftrightarrow\{112\}_\gamma$, $\{001\}_{\alpha''}\leftrightarrow\{110\}_\gamma$

According to the above orientation relationship and the lattice parameters of martensite and the parent phases, the deformation gradient tensor of martensitic transformation (F_p) can be derived, i.e. dx=F_pdX, where dX is the vector before transformation and dx is that after transformation[26]. The transformation strain is derived from the deformation gradient tensor[25]:

$$\varepsilon_{ij}^{00}(p)=\left(F_p^TF_p-I\right)/2 \tag{7}$$

where T denotes the transpose tensor, I is the element tensor. The orientation relationships between the parent phase and martensitic variants are presented in Table 1, and the calculated deformation gradient and transformation strain are presented in Table 2 and Table 3, respectively.

The shear modulus was chosen as μ=29 GPa, and the Possion's ratio was v=0.38[31]. The gradient coefficient and the Landau coefficients cannot be directly derived from experimental results, because we did not find relevant physical parameters. Therefore, these parameters were derived from other similar simulation studies. The gradient energy coefficient was chosen to be 1.6×10^{-8} J/m, which is close to that in Ref. [32]. Assuming that the interface thickness is 10 nm, the interfacial energy is 1.6 J/m^2. A was set as 1.8×10^7 J/m^3. D was chosen to be 1.8×10^9 J/m^3. As the parameters of A and D cannot be found in the literature, adjustment was done before determination in order to obtain appropriate simulation results of martensite microstructure, i.e. clear phase interface and appropriate thickness of variant plates. ΔG_m was different in different cases, in order to provide enough driving force to trigger the transformation. Some parameters were reduced to

Table 1 Orientation relationship between the parent phase and the martensitic variants (V denotes variant)

V	1	2	3	4	5	6	7	8	9	10	11	12
$[100]_{\alpha''}$	$[1\bar{1}1]_\gamma$	$[111]_\gamma$	$[\bar{1}11]_\gamma$	$[\bar{1}\bar{1}1]_\gamma$	$[111]_\gamma$	$[\bar{1}11]_\gamma$	$[\bar{1}\bar{1}1]_\gamma$	$[1\bar{1}1]_\gamma$	$[1\bar{1}1]_\gamma$	$[\bar{1}11]_\gamma$	$[11\bar{1}]_\gamma$	$[111]_\gamma$
$(010)_{\alpha''}$	$(121)_\gamma$	$(1\bar{2}1)_\gamma$	$(\bar{1}\bar{2}1)_\gamma$	$(\bar{1}21)_\gamma$	$(\bar{2}11)_\gamma$	$(211)_\gamma$	$(2\bar{1}1)_\gamma$	$(\bar{2}\bar{1}1)_\gamma$	$(1\bar{1}\bar{2})_\gamma$	$(\bar{1}1\bar{2})_\gamma$	$(112)_\gamma$	$(11\bar{2})_\gamma$
$(001)_{\alpha''}$	$(\bar{1}01)_\gamma$	$(10\bar{1})_\gamma$	$(101)_\gamma$	$(\bar{1}0\bar{1})_\gamma$	$(0\bar{1}1)_\gamma$	$(01\bar{1})_\gamma$	$(011)_\gamma$	$(0\bar{1}\bar{1})_\gamma$	$(110)_\gamma$	$(\bar{1}\bar{1}0)_\gamma$	$(1\bar{1}0)_\gamma$	$(\bar{1}10)_\gamma$

Table 2 Deformation gradient tensor for martensitic variants (DG denotes deformation gradient tensor)

V	DG	V	DG	V	DG
1	$\begin{bmatrix}1.032 & 0.076 & 0.015\\ -0.015 & 0.941 & -0.015\\ 0.015 & 0.076 & 1.032\end{bmatrix}$	5	$\begin{bmatrix}0.941 & 0.015 & 0.015\\ -0.076 & 1.032 & 0.015\\ -0.076 & 0.015 & 1.032\end{bmatrix}$	9	$\begin{bmatrix}1.032 & -0.015 & -0.076\\ -0.015 & 1.032 & 0.076\\ 0.015 & -0.015 & 0.941\end{bmatrix}$
2	$\begin{bmatrix}1.032 & -0.076 & 0.015\\ 0.015 & 0.941 & 0.015\\ 0.015 & -0.076 & 1.032\end{bmatrix}$	6	$\begin{bmatrix}0.941 & -0.015 & -0.015\\ 0.076 & 1.032 & 0.015\\ 0.076 & 0.015 & 1.032\end{bmatrix}$	10	$\begin{bmatrix}1.032 & -0.015 & 0.076\\ -0.015 & 1.032 & -0.076\\ -0.015 & 0.015 & 0.941\end{bmatrix}$
3	$\begin{bmatrix}1.032 & 0.076 & -0.015\\ -0.015 & 0.941 & 0.015\\ -0.015 & -0.076 & 1.032\end{bmatrix}$	7	$\begin{bmatrix}0.941 & 0.015 & -0.015\\ -0.076 & 1.032 & -0.015\\ 0.076 & -0.015 & 1.032\end{bmatrix}$	11	$\begin{bmatrix}1.032 & 0.015 & 0.076\\ 0.015 & 1.032 & 0.076\\ -0.015 & -0.015 & 0.941\end{bmatrix}$
4	$\begin{bmatrix}1.032 & -0.076 & -0.015\\ 0.015 & 0.941 & -0.015\\ -0.015 & 0.076 & 1.032\end{bmatrix}$	8	$\begin{bmatrix}0.941 & -0.015 & 0.015\\ 0.076 & 1.032 & -0.015\\ -0.076 & -0.015 & 1.032\end{bmatrix}$	12	$\begin{bmatrix}1.032 & 0.015 & -0.076\\ 0.015 & 1.032 & -0.076\\ 0.015 & 0.015 & 0.941\end{bmatrix}$

Table 3 Transformation strain tensor for martensitic variants (TS denotes transformation strain tensor)

V	TS	V	TS	V	TS
1	$0.01\begin{bmatrix}3.3 & 3.3 & 1.6\\ 3.3 & -5.2 & 3.3\\ 1.6 & 3.3 & 3.3\end{bmatrix}$	5	$0.01\begin{bmatrix}-5.2 & -3.3 & -3.3\\ -3.3 & 3.3 & 1.6\\ -3.3 & 1.6 & 3.3\end{bmatrix}$	9	$0.01\begin{bmatrix}3.3 & -1.6 & -3.3\\ -1.6 & 3.3 & 3.3\\ -3.3 & 3.3 & -5.2\end{bmatrix}$
2	$0.01\begin{bmatrix}3.3 & -3.3 & 1.6\\ -3.3 & -5.2 & -3.3\\ 1.6 & -3.3 & 3.3\end{bmatrix}$	6	$0.01\begin{bmatrix}-5.2 & 3.3 & 3.3\\ 3.3 & 3.3 & 1.6\\ 3.3 & 1.6 & 3.3\end{bmatrix}$	10	$0.01\begin{bmatrix}3.3 & -1.6 & 3.3\\ -1.6 & 3.3 & -3.3\\ 3.3 & -3.3 & -5.2\end{bmatrix}$
3	$0.01\begin{bmatrix}3.3 & 3.3 & -1.6\\ 3.3 & -5.2 & -3.3\\ -1.6 & -3.3 & 3.3\end{bmatrix}$	7	$0.01\begin{bmatrix}-5.2 & -3.3 & 3.3\\ -3.3 & 3.3 & -1.6\\ 3.3 & -1.6 & 3.3\end{bmatrix}$	11	$0.01\begin{bmatrix}3.3 & 1.6 & 3.3\\ 1.6 & 3.3 & 3.3\\ 3.3 & 3.3 & -5.2\end{bmatrix}$
4	$0.01\begin{bmatrix}3.3 & -3.3 & -1.6\\ -3.3 & -5.2 & 3.3\\ -1.6 & 3.3 & 3.3\end{bmatrix}$	8	$0.01\begin{bmatrix}-5.2 & 3.3 & -3.3\\ 3.3 & 3.3 & -1.6\\ -3.3 & -1.6 & 3.3\end{bmatrix}$	12	$0.01\begin{bmatrix}3.3 & 1.6 & -3.3\\ 1.6 & 3.3 & -3.3\\ -3.3 & -3.3 & -5.2\end{bmatrix}$

the dimensionless form by dividing E=1.8×10^8 J/m^3, i.e. A/E, B/E, C/E, D/E, μ/E, β/E. E was only used to do the operation of dimensionless, which has no physical meaning and its value will not influence the simulation results. The real length of a grid was chosen to be l=3×10^{-8} m. It should be mentioned that there are some assumptions in the present model: no plastic mechanical relaxation, isotropic elastic constants, and isotropic gradient energy. Semi-implicit Fourier-spectral algorithm was applied to solve the evolution equations[33]. A cell containing 129×129×129 cubic grids was used.

2 Results

In order to investigate the growth process of TM, a small cubic single-variant embryo (5×5×5 grids) was set in the system center as the initial condition. Clamped boundary condition was used for solving the mechanical problem, which represents that individual grain was constrained by neighboring grains in polycrystalline materials. If the driving force (ΔG_m) is large enough, the embryo will grow into the parent phase, i. e. transformation starts. As there are 12 variants for α'' martensite, the self-accommodation process becomes relatively complex. In order to reveal the formation mechanism of multi-variant α'' martensite, we chose a part of variants active and other variants are inactive during simulation. Therefore, the growth processes with different variants were obtained.

2.1 Martensite containing 12 variants

At first, all 12 variants are active, and the dimensionless driving force ($-12\Delta G_m/E$) is chosen to be 3.0. It is noted that the driving force is selected to be large enough to trigger the growth of nucleation embryo, smaller driving force will result in vanishing of the embryo, and larger driving force will weaken the effect of self-accommodation. This selection principle is also applied to the following simulation studies. The growth process is shown in Fig. 1, where different colors represent different variants, and the transparent region in the cube represents the parent phase.

At the beginning, the shape of the initially cubic embryo changes, but its size does not obviously increase. Instead, several other variants appear around the embryo surface. Therefore, multi-variant martensite is already formed at the early stage (Fig. 1a). Because obvious transformation strain is accompanied with the transformation, significant internal stress will appear around the embryo[27]. The stress state around the interface triggers the formation of other variants, as stress is one of the driving forces of TMT. As the growth continues, the width of the variant plates increases. At the meantime, new variant plates are formed. The transformation is proceeded by the migration of phase interface between the parent phase and martensite, which is one of the characteristics of first order phase transformation. In addition, the shape of the martensite cluster is irregular during the

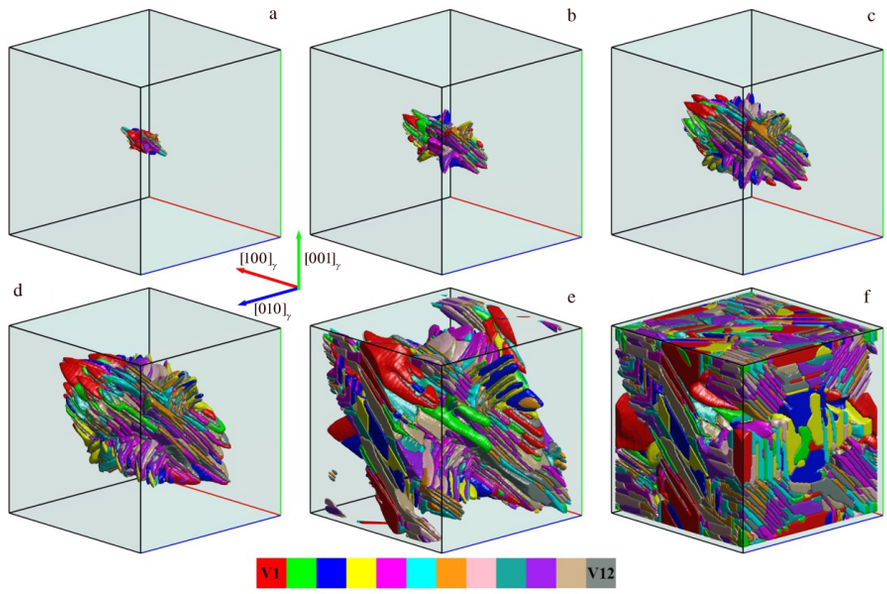

Fig.1 Microstructure evolution of martensite containing 12 variants: (a) t^*=100, (b) t^*=200, (c) t^*=300, (d) t^*=500, (e) t^*=800, and (f) t^*=3000

growing process. Finally, most of the parent phases transform to martensite, but a small amount of them remain unchanged. As the $\gamma \rightarrow \alpha''$ transformation produces a small volume expansion, hydrostatic pressure is generated when the transformation is close to completion in the clamped grain, which hinders the further transformation[34]. After transformation, a simple grain of γ-phase changes into a cluster containing numerous α'' plates with different crystal orientations. Meanwhile, the grain boundaries may still obtain their original characteristics, but in the grain, high density of coherent twinning interface makes the grain more complex (Fig. 1f). As shown in Fig. 1, the plates with different variants intersects with each other, and specific combination of variants cannot be clearly found. Therefore, the number of variants was reduced, and the growth of martensite with a small number of variants was simulated.

2.2 Martensite containing 2 variants

Formation of martensitic twins is the commonest self-accommodation mode. In this section, the growth process of martensite containing 2 variants was simulated, and several combinations of variants were considered. The simulated results are shown in Fig. 2, where the dimensionless driving force is 11.0. For the case of variant 1+variant 8 (V1+V8), a regular twinning band forms at the early stage. There is a certain habit plane between the twinning band and the parent phase. Upon further growth, the band expands on the habit plane, accomplished by lengthening of individual variant plate and forming of new variant plates (Fig. 2a~2c). Three bands appear due to the periodical boundary condition. The habit plane between twinning band of V1+V8 (TB_{V1+8}) and the parent phase is about $(4\bar{4}\bar{7})_\gamma$. The twinning plane is hard to estimate due to high dispersity. The habit plane is the crystal interface between martensite and the parent phase, and the twinning plane is the crystal interface between neighbouring variant plates. These planes can be calculated from the simulated results of microstructure (Fig. 2). V1 can also combine with other variants to form twinning bands, such as TB_{V1+5}, TB_{V1+7} and TB_{V1+12} (Fig. 2e~2g). The habit plane and twinning plane are different for different twinning bands. For example, the habit plane of TB_{V1+12} is about $(\bar{3}50)_\gamma$, the twinning plane is about $(\bar{4}15)_\gamma$. It is well known that the formation of transformation twins can reduce the macroscopic transformation strain, such as

$$\frac{1}{2}\left(\varepsilon_{ij}^{00}(1)+\varepsilon_{ij}^{00}(8)\right)=0.01\begin{bmatrix}-1.0 & 3.3 & -0.9\\ 3.3 & -1.0 & 0.9\\ -0.9 & 0.9 & 3.3\end{bmatrix}$$

$$\frac{1}{2}\left(\varepsilon_{ij}^{00}(1)+\varepsilon_{ij}^{00}(12)\right)=0.01\begin{bmatrix}3.3 & 2.4 & -0.9\\ 2.4 & -1.0 & 0.0\\ -0.9 & 0.0 & -1.0\end{bmatrix}$$

$$\frac{1}{2}\left(\varepsilon_{ij}^{00}(1)+\varepsilon_{ij}^{00}(5)\right)=0.01\begin{bmatrix}-1.0 & 0.0 & -0.9\\ 0.0 & -1.0 & 2.4\\ -0.9 & 2.4 & 3.3\end{bmatrix}$$

$$\frac{1}{2}\left(\varepsilon_{ij}^{00}(1)+\varepsilon_{ij}^{00}(7)\right)=0.01\begin{bmatrix}-1.0 & 0.0 & 2.4\\ 0.0 & -1.0 & 0.9\\ 2.4 & 0.9 & 3.3\end{bmatrix}$$

Using the average transformation strain as the eigen-strain of a single variant, the simulated results are presented in Fig. 2d and 2h. Comparing the results, it can be found that the morphology and habit plane of twinning bands are mainly determined by the average transformation strain. The eigenvalues of the above tensor are not zero, which means that the twinning bands cannot satisfy the condition of invariant plane strain[35]. In addition, the twinning band will stop growing when the increasing internal stress becomes large enough, i.e. the thermoelastic equilibrium state[36] is obtained.

2.3 Martensite containing 3 variants

As shown in the above section, twinning bands still exhibit obvious macroscopic strain. Therefore, the growth process of

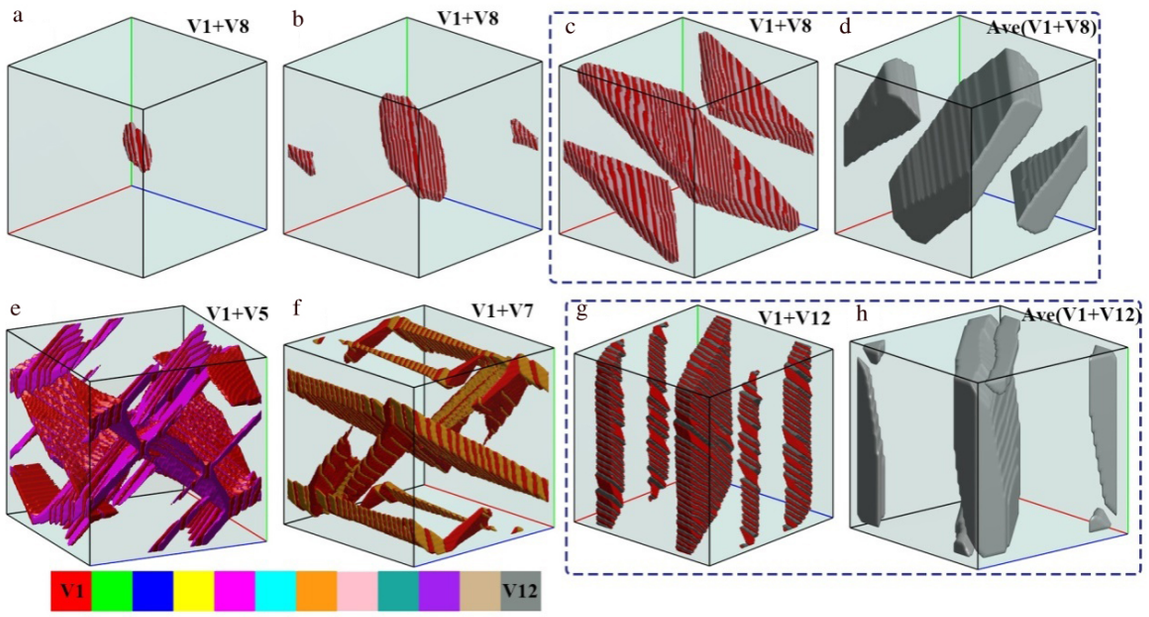

Fig.2 Microstructure evolution of martensite containing 2 variants: (a~c) growth process of V1+V8, (d) single-variant martensite with transformation strain $[\varepsilon_{ij}^{00}(1) + \varepsilon_{ij}^{00}(8)]/2$, (e) martensite of V1+V5, (f) martensite of V1+V7, (g) martensite of V1+V12, and (h) single-variant martensite with transformation strain $[\varepsilon_{ij}^{00}(1) + \varepsilon_{ij}^{00}(12)]/2$

twinning band results in large internal stress around the habit plane, which will be the driving force for other variants. Thus we expanded the number of variants to further reveal the self-accommodation effect. Fig. 3 shows the simulated results of microstructure evolution containing 3 variants. The dimensionless driving force is 6.0. At the early stage, the single-variant embryo grows into a multi-variant cluster with specific shape (Fig. 3a, 3d and 3g), which slightly changes upon growth. Three variants all participate in the self-accommodation process. However, the degree of self-accommodation varies in different cases. The fraction of TB_{V1-8} is larger than that of others in the case of $TM_{V-1-8-10}$, TB_{V5-10} dominates the microstructure of $TM_{V1-5-10}$. However, the density of twinning in the $TM_{V2-6-12}$ is higher than that in other cases, since the three variants can form three types of twinning bands, i.e. TB_{V2-6}, TB_{V2-12} and TB_{V6-12}. This case can be seen as a typical self-accommodation behavior between twinning bands, e.g. the cooperative growth between TB_{V2-6} and TB_{V6-12} (Fig. 4). This cluster of multi-variant martensite presents spear-like morphology, new twinning bands are formed during the thickening process, and the lengthening process is realized by forming plates of different variant alternatively. On the assumption that the fractions of the variants are equivalent, the macroscopic transformation strains of the present three combinations are

$$\frac{1}{3}\left(\varepsilon_{ij}^{00}(1) + \varepsilon_{ij}^{00}(8) + \varepsilon_{ij}^{00}(10)\right) = 0.01\begin{bmatrix} 0.5 & 1.7 & 0.5 \\ 1.7 & 0.5 & -0.5 \\ 0.5 & -0.5 & 0.5 \end{bmatrix}$$

$$\frac{1}{3}\left(\varepsilon_{ij}^{00}(1) + \varepsilon_{ij}^{00}(5) + \varepsilon_{ij}^{00}(10)\right) = 0.01\begin{bmatrix} 0.5 & -0.5 & 0.5 \\ -0.5 & 0.5 & 0.5 \\ 0.5 & 0.5 & 0.5 \end{bmatrix}$$

$$\frac{1}{3}\left(\varepsilon_{ij}^{00}(2) + \varepsilon_{ij}^{00}(6) + \varepsilon_{ij}^{00}(11)\right) = 0.01\begin{bmatrix} 0.5 & 0.5 & 0.5 \\ 0.5 & 0.5 & -1.7 \\ 0.5 & -1.7 & 0.5 \end{bmatrix}$$

It can be found that the macroscopic strain of 3-variants martensite becomes obviously smaller than that of 2-variants martensite.

2.4 Martensite containing 6 variants

Increasing the number of variants to 6, we selected two kinds of combination, and the simulated results are shown in Fig.5. The dimensionless driving force is 4.0. The growth rate is depended on the growth direction. Once a self-accommodated multi-variant block is formed, it will grow rapidly on the habit plane, e.g. TB_{V1-7}+TB_{V1-9}, TB_{V2-9}+TB_{V7-9} and TB_{V1-7}+TB_{V1-10}, as indicated by dotted circles in Fig. 5c. The thickening process of the blocks is usually accomplished by formation of new twinning bands. For the second case, the growth of 3-variants self-accommodated block is absent, but the self-accommodation between different twinning bands can be found, e.g. between TB_{V6-12} and TB_{V4-10} (Fig. 5g). These twinning bands may not possess the same habit plane. In addition, the morphology of the martensite cluster becomes more complex with more variants, which provides more self-accommodation modes to reduce the degree of internal stress. 2D microstructure is usually obtained by experimental methods, and the 2D cross section results are also given in Fig. 5. It can be seen that the 2D results well show the complex self-accommodated microstructure, e.g. the twinning type and the twinning interface. However, the 3D shape of the martensite cluster can be hardly obtained from the 2D results.

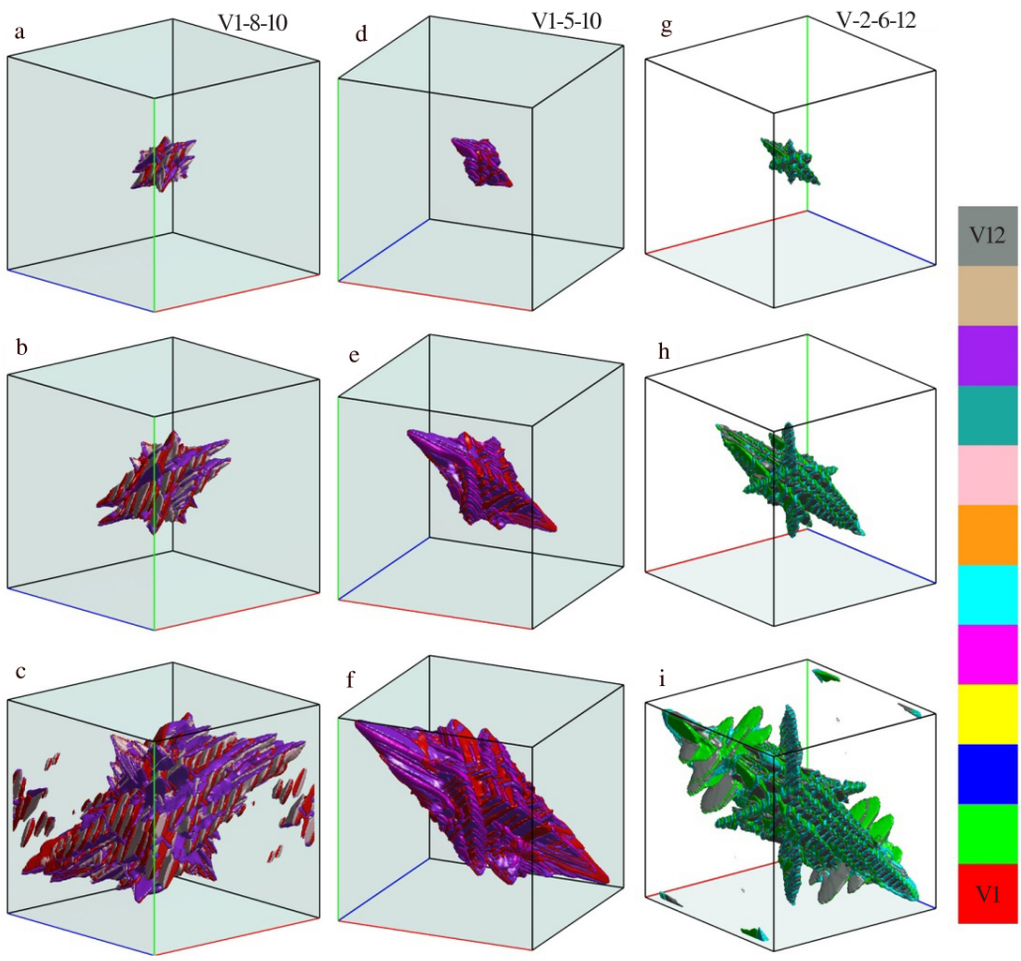

Fig.3 Microstructure evolution of martensite containing 3 variants: (a~c) martensite with V1+V8+V10, (d~f) martensite with V1+V5+V10, and (g~i) martensite with V2+V6+V12

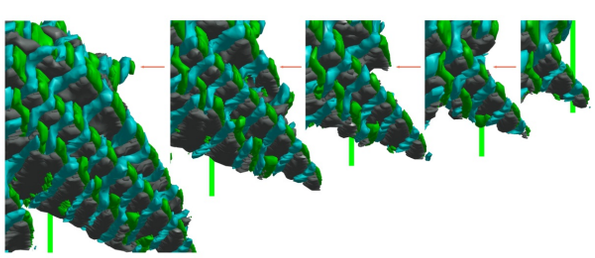

Fig.4 Detailed growth process of a spear-like 3-variants (V2+V6+V12) martensite

3 Discussion

3.1 Formation mechanism of α'' thermoelastic martensite

The above simulation results appropriately reveal the growth characteristics of α'' TM. Firstly, distinct phase interface distinguishes the regions of martensite and the parent phase during the transformation process, which is consistent with the fact that TMT belongs to first order phase transformation[37]. Secondly, in accordance with numerous experimental results in SMAs[7-9,19,20,38,39], the self-accommodation phenomenon is particularly significant. The detailed mechanism is that the internal stress generated by the growth of a variant plate hinders its continuous growth, but favors the appearance of other variant. This effect influences the whole growth process, and finally results in organized multi-variant martensite. Several self-accommodation modes are found in this study, such as twinning bands containing 2 variants, martensite block including 2 types of twinning bands, and simultaneous growth of several multi-variant blocks. It is worth mentioning that these multi-variant martensites are all originated from a single-variant embryo.

$\{130\}_{\alpha''}$ transformation twinning is the commonest twinning mode of α'' martensite, where the variant pairs are V_i and V_{i+1} (i=1, 3, 5, 7, 9, 11)[29]. However, this mode cannot be found in our simulations. The primary reason is that other variant pairs provide smaller macroscopic transformation strain than this mode. For example

$$\frac{1}{2}\left(\varepsilon_{ij}^{00}(1)+\varepsilon_{ij}^{00}(2)\right)=0.01\begin{bmatrix}3.2 & 0.0 & 1.5\\ 0.0 & -5.4 & 0.0\\ 1.5 & 0.0 & 3.2\end{bmatrix}$$

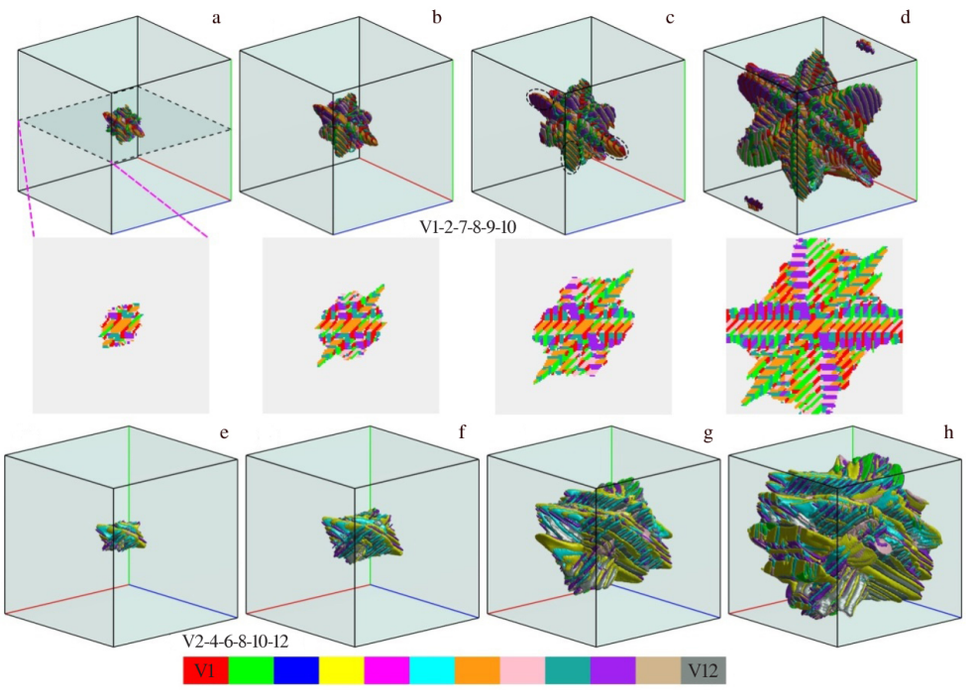

Fig.5 Microstructure evolution of martensite containing 6 variants: (a~d) martensite of V1+V2+V7+V8+V9+V10 and (e~h) martensite of V2+V4+V6+V8+V10+V12

$$\frac{1}{2}\left(\varepsilon_{ij}^{00}(1)+\varepsilon_{ij}^{00}(8)\right)=0.01\begin{bmatrix}-1.0 & 3.3 & -0.9\\ 3.3 & -1.0 & 0.9\\ -0.9 & 0.9 & 3.3\end{bmatrix}$$

The critical driving force for the growth of TB_{1+2} is much higher than that of TB_{1+8}. This discrepancy between the simulation and experimental results can be explained from the point view of deformation gradient tensor. As shown in Table 2, the deformation gradient tensors of $\gamma \rightarrow \alpha''$ TMT are asymmetric, so they are unstable and rigid rotation is expected. However, the combination of F_1 and F_2 is symmetric, i.e.

$$\frac{1}{2}\left(F_1+F_2\right)=\begin{bmatrix}1.032 & 0 & 0.015\\ 0 & 0.941 & 0\\ 0.015 & 0 & 1.032\end{bmatrix}$$

Therefore, it is suggested that the operation of rigid rotation can be replaced by the combination of V_i and V_{i+1} (i=1, 3, ⋯, 11), in order to obtain symmetric deformation gradient tensor. This effect is not considered in the present phase-field model, which uses the symmetric transformation strain tensor as the input parameter.

Assuming that V1 can combine with V2 to form a twinning band, the following step is to determine the twinning plane. Generally speaking, the transformation twinning plane has to satisfy some requirements. Firstly, a crystal plane of the parent phase transforms into two crystal planes of V1 and V2. As these two planes are actually the same plane, i.e. the twinning plane, one requirement is that both planes are equivalent for α'' structure. For example, the original $(010)_\gamma$ plane transforms into $(\bar{1}30)_{V1}$ and $(\bar{1}30)_{V2}$ planes. In addition, the parent plane corresponding to the twinning plane should be a mirror plane[18]. Both conditions were not taken into account in the current phase-field model. As the crystallography requirements for twinning plane and the effect of asymmetric deformation gradient tensor are not considered in the present phase-field model, some of the current simulation results are inconsistent with the experimental results. For example, V1 can combine with V2, V7, V8, V9 or V10 to form twinning plane, from the 2D microstructure of Fig. 5d. However, V1 cannot combine with V7 and V10 from the view point of crystallography[18]. Therefore, a more rigorous phase-field model of martensitic transformation should consider the crystallography theory of martensitic transformation, besides the thermodynamic and kinetic theories.

3.2 Influence of thermoelastic martensite on the plastic behavior

Besides the specific shape memory effect and superelastic behavior, the plastic deformation of SMAs is also different from that of conventional structural materials. After transformation, the microstructure consists of numerous fine variant plates and high density of twinning interface. As one of the driving forces, stress will change the relative stability of martensitic variants. In the process of stress loading, some variants become more stable than others. Therefore, variant rearrangement will appear upon deformation[20,40]. The deformation stage of variant rearrangement contributes to ductility improvement[17], anomalous stress-strain curve[20] and relatively low yield strength[41]. This stage is different from conventional plastic deformation. Appreciable macroscopic strain is generated without obvious dislocation slip plasticity. Thus, the subsequent plastic flow stage still maintains

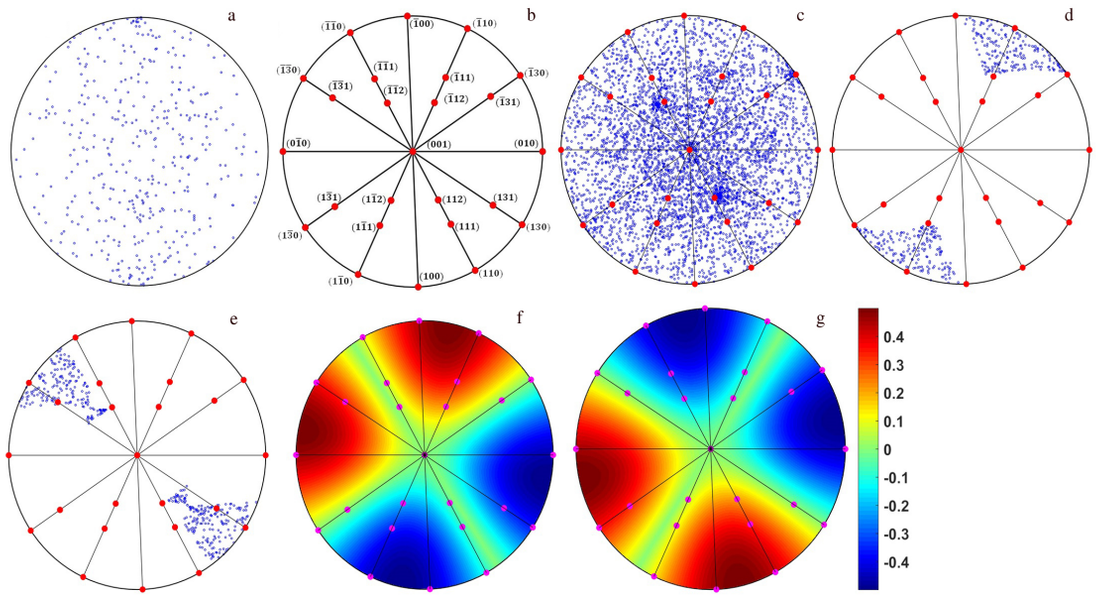

Fig.6 IPF of 400 γ-phase random orientation grains (a); standard stereograph of monoclinic α'' structure (b); IPF of α''-phase after transformation from Fig. 6a (c); IPFs of α'' structure after variant rearrangement upon uniaxial compressive (d) and tensile (e) deformations; calculated Schmid factor for $(1\bar{3}0)[\bar{3}\bar{1}0]$ (f) and $(130)[3\bar{1}0]$ twinning modes under uniaxial tension (g)

considerable ductility.

Assuming that the multi-variant grains change to single-variant grains after variant rearrangement, the favored variant will possess the maximum strain along the loading direction[29]. As a result, crystallographic texture may arise in polycrystalline specimen. For the case of uniaxial deformation, assuming a γ-phase polycrystalline specimen containing 400 grains of random orientation, the inverse pole figure (IPF) along the deformation direction is shown in Fig. 6a. After transformation, a γ orientation will produce 12 α'' orientations. Assuming that the multi-variant martensite consists of all 12 variants, the IPF result is shown in Fig. 6c. After variant rearrangement, only favored variant remains, the obtained IPFs for uniaxial tension and compression are shown in Fig. 6d and 6e. It can be found that significant textures are developed, and both results are in good agreement with experimental results in Ref. [29, 42]. In addition, the macroscopic strains corresponding to variant rearrangement are 0.052 and −0.062 for tensile and compressive deformation, respectively, close to the reversible strain for shape memory effect obtained by experiments[14, 43]. Fig. 6f and 6g show the calculated Schmid factors for two deformation twinning modes, i. e. $(1\bar{3}0)[\bar{3}\bar{1}0]$ and $(130)[3\bar{1}0]$, which are the commonest deformation twinning modes in α-U considering the similarity between the α and α'' structures. Combining the Schmid factor with the texture, it can be found that low Schmid factor commonly exists in the textured grains, which means that after rearrangement, the grains become more difficult to realize the $\{130\}<3\bar{1}0>$ twinning. Therefore, the obtained texture will influence the following deformation process.

4 Conclusions

1) Driven by minimization of elastic strain energy, the self-accommodation effect results in multi-variant martensite throughout the growth process.

2) For α'' thermoelastic martensite, twinning band is the simplest self-accommodation mode. An individual single-variant embryo can grow into a martensite cluster containing several twinning bands, and different twinning bands grow up collaboratively to further reduce the macroscopic transformation strain.

3) Besides minimizing macroscopic transformation strain, the asymmetric deformation gradient tensor and interface compatibility notably influence the type of transformation twins. The variant rearrangement process results in obvious texture development, which will affect the subsequent plastic flow process.

References

1 Otsuka K, Kakeshita T. *MRS Bulletin*[J], 2002, 27(2): 91
2 Otsuka K, Shimizu K. *International Metals Reviews*[J], 1986, 31(3): 93
3 Chen H, Xiao F, Liang X *et al*. *Acta Materialia*[J], 2019, 177: 169
4 Otsuka K, Wayman C M. *Shape Memory Materials*[M]. Cambridge: Cambridge University Press, 1998
5 Yin F, Sakaguchi T, Tian Q *et al*. *Materials Transactions*[J], 2005, 46(10): 2164
6 Szczerba M J, Chulist R. *Acta Materialia*[J], 2015, 85: 67
7 Nishida M, Nishiura T, Kawano H *et al*. *Philosophical Magazine*[J], 2012, 92(17): 2215

8 Soejima Y, Motomura S, Mitsuhara M *et al*. *Acta Materialia*[J], 2016, 103: 352

9 Chai Y W, Kim H Y, Hosoda H *et al*. *Acta Materialia*[J], 2009, 57: 4054

10 Jin Y M, Artemev A, Khachaturyan A G. *Acta Materialia*[J], 2001, 49: 2309

11 Qiu Z C, He L F, Xiao D W *et al*. *Rare Metal Materials and Engineering*[J], 2014, 43(11): 2829 (in Chinese)

12 Guo Y K, Shuai M B, Zou D L *et al*. *Rare Metal Materials and Engineering*[J], 2018, 47(5): 1459 (in Chinese)

13 Xiao D W, He L F, Qiu Z C *et al*. *Rare Metal Materials and Engineering*[J], 2018, 47(1): 363 (in Chinese)

14 Jackson R J, Johns W L. *Temperature-Induced Shape Memory in Polycrystalline Uranium-Base Niobium Alloys: Characterization* [R]. Colorado: The Dow Chemical Company Rocky Flats Division, 1970

15 Vandermeer R A, Ogle J C, Snyder Jr W B. *Scripta Metallurgica* [J], 1978, 12: 243

16 Vandermeer R A. *Acta Metallurgica*[J], 1980, 28: 383

17 Eckelmeyer K H, Romig A D, Weirick L J. *Metallurgical Transactions A*[J], 1984, 15: 1319

18 Hatt B A. *Journal of Nuclear Materials*[J], 1966, 19: 133

19 Jenkins B A, Edmonds D V. *Materials Science Forum*[J], 1990, 56-58: 323

20 Field R D, Thoma D J, Dunn P S *et al*. *Philosophical Magazine* [J], 2001, 81(7): 1691

21 Steinbach I. *Modelling and Simulation in Materials Science and Engineering*[J], 2009, 17: 73 001

22 Zhang B, Zhao Y H, Wang H *et al*. *Rare Metal Materials and Engineering*[J], 2019, 48(9): 2835 (in Chinese)

23 Zhang J H, Xu D S, Teng C Y *et al*. *Rare Metal Materials and Engineering*[J], 2020, 49(3): 939 (in Chinese)

24 Zhao X T, Shang S, Zhang T X *et al*. *Rare Metal Materials and Engineering*[J], 2020, 49(11): 3709 (in Chinese)

25 Gao Y, Zhou N, Wang D *et al*. *Acta Materialia*[J], 2014, 68: 93

26 Mamivand M, Zaeem M A, Kadiri H E. *Acta Materialia*[J], 2015, 87: 45

27 Cui S S, Wan J F, Zuo X W *et al*. *Materials and Design*[J], 2016, 109: 88

28 Wang Y, Khachaturyan A G. *Acta Materialia*[J], 1997, 45(2): 759

29 Field R D, Brown D W, Thoma D J. *Philosophical Magazine*[J], 2005, 85(23): 2593

30 Carpenter D A, Vandermeer R A. *Journal De Physique*[J], 1982, 43: 4

31 Souza P R. *Ultrasonic Time-of-Flight Measurements on Binary U-6Nb Cubes*[R]. Livemore: Lawrence Livemore National Laboratory, 2005

32 Mamivand M, Zaeem M A, Kadiri H E *et al. Acta Materialia*[J], 2013, 61: 5223

33 Chen L Q, Shen J. *Computer Physics Communications*[J], 1998, 108: 147

34 Malik A, Yeddu H K, Amberg G *et al*. *Materials Science & Engineering A*[J], 2012, 556: 221

35 Wayman C M. *Journal of the Less Common Metals*[J], 1972, 28: 97

36 Olson G B, Cohen M. *Scripta Metallurgica*[J], 1975, 9: 1247

37 Ortín J, Planes A. *Acta Metallurgica*[J], 1989, 37(5): 1433

38 Delville R, Kasinathan S, Zhang Z *et al*. *Philosophical Magazine* [J], 2010, 90: 177

39 Nishida M, Matsuda M, Yasumoto Y *et al*. *Materials Science and Technology*[J], 2008, 24(8): 884

40 Liu Y, Xie Z, Humbeeck J V *et al*. *Acta Materialia*[J], 1998, 46(12): 4325

41 Brown D W, Bourke M A M, Clarke A J *et al*. *Journal of Nuclear Materials*[J], 2016, 481: 164

42 Tupper C M, Brown D W, Field R D *et al*. *Metallurgical and Materials Transactions A*[J], 2012, 43(2): 520

43 Vandermeer R A, Ogle J C, Northcutt W G. *Metallurgical and Materials Transactions A*[J], 1981, 12(5): 733

U-Nb形状记忆合金热弹性马氏体相变的相场模拟

崔书山，张　雷，法　涛

(中国工程物理研究院 材料研究所，四川 江油 621907)

摘　要：U-Nb形状记忆合金具有优异的抗腐蚀性和力学性能，其中亚稳α″相的典型微观组织为多层级孪晶马氏体。利用相场法模拟α″相热弹性马氏体的形成过程。结果表明，在弹性应变能最小化的驱动下，获得了多种自协调马氏体组织，也发现了多种自协调模式。对比本研究模拟结果和文献中的实验结果，认为相变变形梯度矩阵的反对称性和界面兼容性显著影响变体结对和孪晶面。另外，基于变体重排过程，预测了相变态组织在变形初期的织构演化。

关键词：U-Nb合金；马氏体相变；相场模型

作者简介：崔书山，男，1992年生，博士，中国工程物理研究院材料研究所，四川 江油 621907，电话：0816-3626743，E-mail：cuishushan@caep.cn